LAWRENCE
LIVERMORE
NATIONAL
LABORATORY

UCRL-JRNL-207382

Saturation of Stimulated Brillouin Backscattering in Two-dimensional Kinetic Ion Simulations

B. I. Cohen, L. Divol, A. B. Langdon, E. A. Williams

October 20, 2004

Physics of Plasmas

Saturation of Stimulated Brillouin Backscattering in Two-dimensional Kinetic Ion Simulations

B.I. Cohen, L. Divol, A.B. Langdon, and E.A. Williams

University of California Lawrence Livermore National Laboratory

P.O. Box 808, Livermore, CA 94551

Two-dimensional simulations with the BZOHAR hybrid code (kinetic PIC ions and Boltzmann fluid electrons) have been used to investigate the saturation of stimulated Brillouin backscatter (SBBS) instability. The simulation physics model provides a first-principles description of several nonlinearities that affect SBBS saturation: wave breaking and ion trapping (and the associated nonlinear frequency shift of the ion wave and nonlinear modification of the ion collisionless kinetic dissipation), two-ion-wave decay instability, harmonic generation, and pump depletion. The simulations address the interplay of these nonlinearities in affecting SBBS saturation as a function of the population of resonant ions, which is controlled by ZT_e/T_i in a single ion species plasma. The competition of various saturation mechanisms and the contrast between one-dimensional and two-dimensional physics are of particular interest. We also examine the role of ponderomotive filamentation in these simulations. The peak reflectivities in two dimensions are less than in one dimension. The two-dimensional reflectivities and ion wave amplitudes in simulations with strong backscatter relax to very small values in times corresponding to less than 40 ps in experimentally relevant conditions, while one-dimensional simulations with the same physical parameters sustain high reflectivities and

concomitant ion wave amplitudes for much longer times. Two-dimensional physics facilitates higher ion wave dissipation rates that account for the relaxation and suppression of SBBS. After the crash of the SBBS in two dimensions, the longitudinal ion velocity distribution function supports significant ion Landau damping (because of the combination of finite negative slope and a large tail of energetic ions), which is shown in the simulations to be the critical element in the continued suppression of SBBS after the crash.

PACS: 52.38.-r 52.65.Rr

I. INTRODUCTION

There is longstanding interest in the nonlinear interaction of intense, coherent electromagnetic waves with high-temperature fusion plasmas. The basic science of laser-plasma interactions is complex and interesting, and nonlinear laser-plasma interactions are very important in inertial confinement fusion (ICF) applications. This study addresses some of the physics affecting the nonlinear saturation of stimulated Brillouin scattering, a process in which laser light is scattered by an ion acoustic wave driven by the ponderomotive force of the incident and scattered electromagnetic waves. This work extends work published in Ref. 1 in several ways. One-dimensional (1D) and two-dimensional (2D) hybrid (PIC ions + Boltzmann fluid electrons) simulations have been performed with the BZOHAR[1] simulation code investigating the saturation of stimulated Brillouin backscattering (SBBS). Several nonlinearities contribute to the saturation of SBBS: ion trapping, wave breaking, pump depletion, two-ion-wave decay instability and nonlinear ion Landau damping, harmonic generation, and driven ion-acoustic turbulence. We observe that SBBS reflectivities saturate at significantly lower amplitudes in the 2D simulations than do SBBS reflectivities in 1D simulations. The decay of the SBBS ion wave (IAW) into longer wavelength ion waves and quasi-modes (induced scattering by ions) in 2D is active when the SBBS crashes. After the SBBS crash in 2D there is substantial ion wave dissipation coming from the ion velocity distribution, which has a substantial population of ions in the tail and is less flattened and not inverted as in 1D. Ion mode coupling in 2D can provide additional dissipation when the ion waves have finite amplitude. By doing several simulations initialized with SBBS-modified ion velocity distribution functions that have been extracted from 1D and 2D simulations in

which there was high SBBS activity, we have been able to derive additional insights that support the analysis and interpretation of the results.

There is evidence of self-focusing or filamentation and forward SBS for $ZT_e/T_i>>1$ after SBS backscatter saturates in the 2D simulations. Because the SBS backscatter occurs early in the simulation, saturates, and crashes, the backscatter is largely independent of the subsequent forward scattering and self-focusing or filamentation.

The research reported here fits into the context of previous research on the saturation of stimulated Brillouin backscatter in a high-temperature, collisionless plasma as follows. This investigation undertakes a direct comparison of 1D and 2D SBS saturation in a model with kinetic ions and fluid electrons. A systematic parameter study is reported in which the relative ion temperature is varied, which controls the ion Landau damping and influences the convective gain of SBBS. The important role of a secondary instability, viz., the nonlinear scattering of the SBBS primary ion wave into other ion waves[1-4] and heavily damped ion quasi-modes,[4] features prominently in differentiating the 1D and 2D physics results. Earlier work on the theory and simulation of SBS has shown the importance of wave breaking and ion trapping,[1-3,5-11] harmonic generation,[12,13,14] and secondary instability of the ion wave.[1-4] In some recent 1D simulations of SBBS, the inclusion of kinetic electrons has made a difference in the saturation of SBBS.[15,16]

The rest of the paper is organized as follows. Section II briefly reviews the BZOHAR simulation model. In Section III we present simulations of stimulated Brillouin scattering and ponderomotive self-focusing or filamentation, and accompanying analysis and interpretation. Conclusions are given in Section IV.

II. BZOHAR SIMULATION MODEL

BZOHAR uses an efficient 2D hybrid simulation model introduced in Ref. 1 with particle ions and Boltzmann fluid electrons. A temporal-enveloped wave equation with fluid electron current determines the electromagnetic vector potential A_z (linearly polarized here perpendicular to the simulation plane and undamped):

$$-i2\omega_0 \frac{\partial}{\partial t} A_z - \omega_0^2 A_z - c^2 \nabla^2 A_z = \omega_{pe}^2 A_z \qquad (1)$$

Poisson's equation with Boltzmann electrons to remove fast electron time scales yields the electric potential ϕ:

$$\nabla^2 \phi = 4\pi e(\sum_s Z_s n_s - n_0 e^{e\phi/T_e}) \qquad (2a)$$

where $n_e = n_0 e^{e\phi/T_e}$ and

$$\Phi(\vec{x},t) = \phi(\vec{x},t) + \frac{m_e}{2}(eA_z/m_e c)^2 \qquad (2b)$$

and the sum in (2a) is over ion species. The ions are advanced as superparticles with equations of motion:

$$d\vec{x}/dt = \vec{v}, m_s d\vec{v}/dt = q_s(\vec{E} + \vec{v} \times \vec{B}/c) \qquad (3)$$

The incident laser propagates in x from left to right and enters the plasma at x=0. The boundary conditions are periodic in y and open/bounded in x (outgoing electromagnetic waves, f_s=ϕ=0, and the ions are confined by an imposed potential barrier).

In the simulations, a large-amplitude electromagnetic pump wave was incident from the left and a very small amplitude electromagnetic backscatter seed wave was incident from the right. The incident seed wave was broadband in frequency, $\omega\omega_{FM}\omega 3\omega_s$, and $v_{seed}/v_e=10^{-3}$, where ω_s is the SBBS IAW frequency, v_{seed} is the electron oscillation velocity in the electromagnetic seed wave, and $v_e=(T_e/m_e)^{1/2}$ is the electron thermal speed. In the

simulations described here the influence of having a backscatter seed as compared to no seed whatever (the backscatter then grew from ion particle discreteness noise that served as a source for both density and current fluctuations) was that the backscatter peak reflectivities were no more than 20% enhanced with the seed present.

III. SIMULATIONS OF STIMULATED BRILLOUIN SCATTERING AND PONDEROMOTIVE FILAMENTATION

A. Simulation parameters

Our 2D baseline simulation parameters are as follows: $6000\Delta x \times 256\Delta y$, $L_x=192\lambda_0$, $L_y=16\lambda_0$, $k_0\Delta x=0.2$, $\omega_{pi}\Delta t=0.2$, $\omega_s\Delta t=0.08$, $\omega_s t=414 \sim 40$ps, $n_e/n_c=0.1$, Be plasma ($Z=4$, $A=9$), $\lambda_e=\Delta x$, $m_h/m_e=1836$, $ZT_e/T_i=2$ to 16, $T_e=2$ keV, collisionless (approximately), $v_0/v_e=0.2$ ($I_0 \sim 1.6\times10^{15}$ W/cm^2 for $\lambda_0=1/3$ μm), $v_{seed}/v_e=0.001$, number of ion superparticles $N_i= 10^5 \times N_y$ (2D), $10^3 \times N_x$ (1D), where ω_{pi} is the ion plasma frequency, ω_s is the ion acoustic frequency associated with the backscatter, λ_e is the electron Debye length, λ_0 is the incident laser wavelength, $T_{e,i}$ are the electron and ion temperatures, $L_{x,y}$ are the system dimensions, $\Delta x \approx \Delta y/2$ are the grid sizes, I_0 is the laser intensity incident from the left, n_e is the electron density, n_c is the critical electron density, and t is the typical duration of the simulation. In these simulations $k_y=\pm(0,1,2,3)\times 2\pi/L_y$ for the electromagnetic wave field, and the full complement of 2D modes for the electrostatic potential was used. The simulations with this restriction on k_y for the electromagnetic wave field allow for forward SBS, filamentation, Gaussian beam propagation and self-focusing at least in a limited way while preventing sidescatter SBS from being artificially preferred over backscatter because of the periodic boundaries in y. For the laser and plasma parameters chosen and the system size used, the linear theory of stimulated

Brillouin backscattering and ponderomotive filamentation yields the following expressions for the intensity gain of scattered waves in a uniform plasma with length L_x when the instability threshold conditions are satisfied.[7,17,18] For stimulated Brillouin backscatter and $T_i/ZT_e << 1$,

$$G_{SBS} = \frac{1}{8}\frac{v_0^2}{v_e^2}\frac{n_e}{n_c}\frac{\gamma_s}{\nu_s}\frac{\gamma_0 L_x}{v_g(1+k^2\lambda_e^2)} \approx 0.5\frac{\gamma_s}{\nu_s} \tag{4}$$

for the intensity gain exponent with a heavily damped IAW, and the IAW damping rate ν_s satisfies $\nu_s > 2\gamma_{sbs}(c_s/c)^{1/2}$ to avoid absolute instability, where $\gamma_{SBS}^2 = \omega_s\omega_{pe}^2 v_0^2/16\omega_0 v_e^2$ and $v_g = k_0 c^2/\omega_0$. For ponderomotive filamentation

$$G_{fil} = \frac{1}{4}\frac{v_0^2}{v_e^2}\frac{1}{1+T_i/ZT_e}\frac{n_e}{n_c}\frac{\gamma_0 L_x}{v_g} \approx 1.2\frac{1}{1+T_i/ZT_e} \tag{5}$$

for the scattered intensity gain exponent. Ponderomotive filamentation of an incident plane wave pump requires that the transverse plasma dimension be wide enough to accommodate the long wavelength modes required for instability, namely[17]

$$\left(\frac{2\pi}{k_0 L_\perp}\right)^2 \ge \frac{k_\perp^2}{k_0^2} \ge \frac{1}{2}\frac{\omega_{pe}^2}{k_0^2 c^2}\frac{v_0^2}{v_e^2}\frac{1}{1+T_i/ZT_e} \tag{6}$$

In a series of four simulations of SBBS we varied the number of particles per cell in order to understand noise issues due to particle statistics: N/cell=6, 13, 25, and 50. The remaining parameters were held fixed: $4000\lambda_0 \times 256\lambda_0$, $\lambda_e=\lambda_0$, $L_x=192\lambda_0$, $L_y=16\lambda_0$, Be plasma (Z=4, A=9), m_h/m_e=1836, T_e=2 keV, ZT_e/T_i=9.6, v_0/v_e=0.2, v_{seed}/v_e=0.01, n_e/n_c=0.1, $\omega_s t$=414 ~ 40ps. Only k_y=0 modes were retained in the light waves, and the incident pump laser was a plane wave. The phenomena studied here, viz., the nonlinear saturation of stimulated Brillouin backscatter involves a complex interplay of highly nonlinear, time-dependent, collisionless Vlasov phenomena and parametric instabilities. Ions are

trapped and detrapped in electric potential wells that vary in time and space. The result is that the time history of a macroscopic observable such as the reflectivity (ratio of reflected electromagnetic wave power to incident power measured where the incident pump wave enters the plasma and integrated over the transverse dimension) can be strongly time-dependent and bursty. The reflectivity may or may not approach a steady state in a given simulation. Furthermore, if the reflectivity time history is bursty and has chaotic features, then the detailed time history may not converge as the number of particles is increased, although the time-asymptotic reflectivity does tend to converge. Nevertheless, comparison of the time histories of the reflectivities (as in Figure 1) gives us estimates of the shot noise due to particle discreteness and the signal-to-noise characteristics. For the parameters considered, we concluded that in 2D simulations the number of particles per cell N/cell=6 was inadequate while N/cell≥16 gave adequate signal-to-noise, e.g., the noise was less than 5% of the peak of the coherent component of the signal in the reflectivity or the electric potential measured by a probe. The time-asymptotic reflectivities converged, but the detailed time histories did not. In light of this we adopted the following operational philosophy. We froze the numerical parameters in the series of simulations, i.e., the number of particles per cell, the time step, and the spatial resolution, such that numerical dispersion was small and adequate signal-to-noise was guaranteed when SBBS reflectivities exceeded a few percent, and then varied one physics parameter at a time to study the influence of that physics parameter on the observables in the absence of changing any of the numerical parameters.

Among the omissions in our model are kinetic electron effects and ion-ion collisions. Ion-ion collisions can relax the modifications in the ion velocity distribution

function $f_i(\mathbf{v})$ due to trapping. For example, we expect that collisions will restore $f_i(\mathbf{v})$ to a Maxwellian over a timescale equal to the characteristic collision time of the most

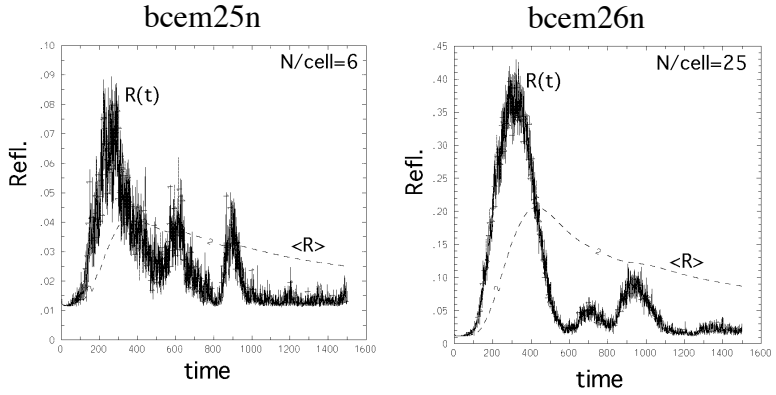

Figure 1. Stimulated Brillouin backscatter (SBBS) instantaneous reflectivity R(t) and the cumulative time-averaged reflectivity <R> up to time t ($\omega_0 t$=0.3) from simulations with (a) N/cell=6 and (b) N/cell=25.

energetic resonant ions. A 2D simulation model including ion-ion collisions in SBS will be the subject of a future investigation. 1D SBBS PIC simulations with strong collisions have been examined in Ref. 19. If the plasma density is tenuous and the resonant ions sufficiently energetic, the collision timescale can exceed the timescales of the SBS saturation, which is the case for the simulations reported here. For ion energies appropriate for ions resonant with the SBBS ion acoustic wave and heated by the SBBS, the characteristic ion collision rate is given by $\nu_i \approx 4.8\times10^{-8} s^{-1} Z^4 n_i(cm^{-3}) \ln\Lambda / [(m_i/m_h)^{1/2}(ZT_e(eV))^{3/2}]$, which for our parameters gives $\nu_i \approx 3\times10^{10} s^{-1}$ or a collision time approximately equal to 30 ps. Our simulations typically corresponded to 40 ps in duration, and saturation of strong SBBS occurred in times corresponding to ~15 ps. This simple estimate of the collision time hides the actual complexity: the ions are strongly heated by the SBBS in the strong-SBBS examples

considered here, and a significant hot-ion, non-Maxwellian tail in the longitudinal velocity distribution is formed. The relevant collision time is that required to relax the non-Maxwellian features, which are observed in our $ZT_e/T_i = 16$ simulation shown later in the paper to extend approximately twice the ion wave trapping width $v_T = \sqrt{Ze\phi/m_i} \sim v_i \equiv \sqrt{T_i/m_i}$ above and below c_s in that simulation and to higher energies in a tail that is formed. Collisional relaxation in this case requires relaxing a substantial fraction of the heated distribution function. Our conclusion is that the neglect of ion-ion collisions over the timescales of the simulations considered here is probably marginally valid, but future work should include a more careful examination of the importance of collisions; and ion-ion collisions should be incorporated in simulating longer timescales.

The inclusion of kinetic electron effects in SBS is likewise of interest[15,16] but is beyond the scope of the investigations reported here which focus on kinetic ions and 2D effects. Electron trapping of low-velocity electrons, $v \sim c_s << (T_e/m_e)^{1/2}$, where $c_s=(ZT_e/m_e)^{1/2}$ is the sound speed, readily occurs in an ion acoustic wave. The electron trapping frequency is larger by $(m_i/Zm_e)^{1/2}$ than the ion trapping frequency, and in consequence electron trapping will precede ion trapping. The electron trapping in an IAW induces a nonlinear frequency shift that is opposite in sign (the shift is positive) to that due to the trapped ions.[20] The effects of electron trapping on the electron Landau damping for an IAW are expected to locally weaken the damping where flattening of the velocity distribution occurs. Recent 1D simulations have shown that including kinetic electrons leads to results for SBBS saturation that differ from those with a Boltzmann fluid electron

model.[15,16] For a given IAW amplitude, the nonlinear ion dynamics is an independent physical effect and is the focus of this study.

B. Nonlinearities Affecting Stimulated Brillouin Scattering

There are several important nonlinearities supported by our model. Ion trapping is a robust nonlinearity in our SBS simulations. Ion trapping produces a hot-ion tail in $f_i(\mathbf{v})$, detunes the SBS resonance by inducing a frequency shift,[1,3,4,8] and flattens and heats $f_i(\mathbf{v})$ non-uniformly in space and anisotropically, which modifications persist after the ion wave damps.[11] Harmonic generation $\mu |e\delta/T_e|^2$ appears transiently at high IAW amplitudes.[12-14] Two-ion-wave decay instability can occur in which the primary SBS ion wave is driven at a frequency above its nonlinear normal mode frequency (e.g., due to trapping), which allows it to decay to two half-harmonic ion waves propagating slightly obliquely to the primary ion wave.[1-4] In 2D, the primary SBS ion wave also can scatter into an obliquely propagating ion wave and thermal ions that are resonant with the ponderomotive beat-wave potential of the primary and daughter IAWs (nonlinear ion Landau damping (NLLD) or induced scattering by ions). For strong backscatter with significant reflectivities, the incident pump light wave can be depleted.

Parametric decay of the SBBS primary ion wave into two longer wavelength ion acoustic modes can occur: $\omega_{s1} = \omega_{s2} + \omega_{s3}$. A treatment of ion-wave decay in two spatial dimensions was presented in Refs. 1 and 4, and evidence of its occurrence in simulations is given in Refs. 1-3. The most unstable modes have $k_\parallel \sim k_{s1}/2$ with growth rate $\gamma \sim \gamma_{s1}$ $(\delta n_e/n_e)_{s1}/4$ and lowest threshold: $|\delta n_{e,s1}/n_e \rhd 4(\gamma_{s2}\gamma_{s3}/\omega_{s1}^2)^{1/2}$, where γ_{s2} and γ_{s3} are the damping rates of the IAW decay products and δn_{e1} is the amplitude of the electron number density associated with the primary IAW. There have been experimental

observations of the two-ion-wave decay in LULI experiments reported by Bandulet *et al*[21] and in Trident experiments reported by Niemann *et al*.[22] The two-ion wave decay accompanied ion trapping in the simulations reported in Refs. 1, 2, and 3. Analysis of the dispersion relation for the two-ion-wave decay (illustrated in Figure 2) has indicated that, owing to the dispersion of the IAW, circumstances for driving the two-ion-wave decay are much improved when the primary IAW is driven above its linear normal-mode frequency.[4] This makes frequency matching for the resonant three-wave decay much easier to satisfy. Because the ion trapping leads to a nonlinear downward shift in the IAW normal mode frequencies for ion waves with phase velocities nearly parallel to the primary IAW (including the two-ion-wave decay product waves which are observed with $k_{\perp} << k_{\parallel}$) while the driving frequency for the SBBS IAW is fixed by the parametric amplification from deeper into the plasma where the IAW is smaller in amplitude and linear in its behavior, the trapped-ion negative frequency shift facilitates the frequency-matching conditions for the two-ion-wave decay by offsetting the dispersive corrections due to finite $k\lambda_e$. Increasing the primary IAW frequency shift permits resonant decay at larger angles to the primary IAW. In two spatial dimensions resonant IAW decay is allowed over a range of nonlinear frequency shifts.

Both of the IAW decay product waves need not be linear normal modes if the coupling is strong enough. Williams[4] extended the analysis of the two-ion-wave decay to the kinetic regime to allow for strongly damped decay waves. The decay process is then more properly described as induced scattering of the primary ion wave by ions, which can spread the ion wave spectrum in 2D and dissipate ion wave energy into ion thermal energy. There is a continuous transition between two-ion-wave decay and NLLD

determined by the Landau damping of the IAW decay products. In 2D, the scattering of finite-amplitude ion waves into obliquely propagating thermal ions and lower-frequency ion waves can occur and is described by the following resonance condition:

$$\omega_{s1} = \omega_{s2} + \vec{k} \cdot \vec{v} \quad \omega_{s1} \approx \omega_{s2} \approx (k_{s1} \approx k_{s2}) c_s = \left| \vec{k}_{s1} \approx \vec{k}_{s2} \right| v_{res} \tag{8}$$

Thus, the resonant ion velocity is given by

$$v_{res} = \approx c_s, \approx = (k_{s1}^2 + k_{s2}^2 \approx 2k_{s1}k_{s2})^{1/2} / (k_{s1}^2 + k_{s2}^2 \approx 2k_{s1}k_{s2} \cos \approx)^{1/2} \tag{9}$$

where $\approx$ is the angle between the primary IAW wave vector and the scattered daughter IAW. For 1D, $\approx$=0 and $\approx$=1, so that $v_{res}=c_s$ and there are few resonant ions if ZT_e/T_i>>1,

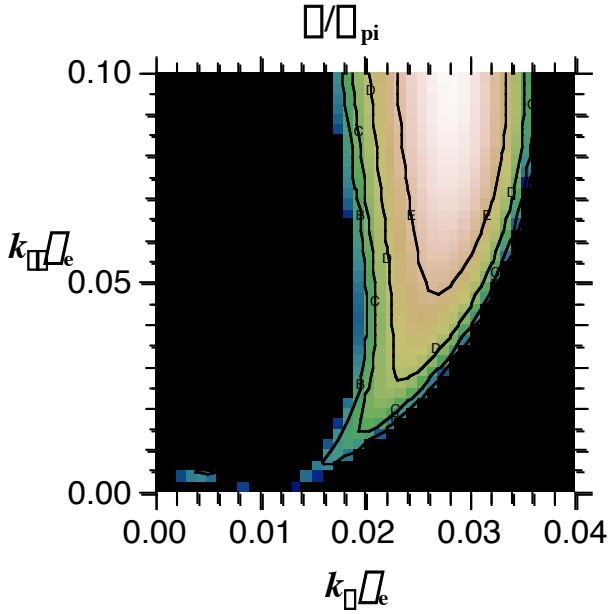

Figure 2. Contours of the two-ion-wave decay growth rates normalized to ω_{pi} are plotted as functions of $k_{\parallel}$ (parallel to the propagation of the primary IAW) and $k_{\perp}$ for primary IAW amplitude $\delta n_e / n_e = 0.05, k_{s1}\lambda_e = 0.2, \omega_{s1} = 1.082\omega_{res}$.

because c_s>>v_i. In 2D with $\approx$≠0, then $\approx$<<1 and v_{res}<<c_s is allowed; and NLLD can involve much more numerous thermal ions. Thus, it is relatively difficult for induced scattering of the primary IAW by ions to occur in 1D, but it is much easier in 2D.

C. Stimulated Brillouin Backscatter Simulation Results

The 2D peak SBBS reflectivities are less than in 1D simulations and crash to much lower amplitudes when there is strong SBBS. The Gaussian beams have higher peak intensities and slightly higher reflectivities than do 2D plane-wave beams. Figure 3 shows a comparison of the reflectivity time histories from three simulations with $ZT_e/T_i = 16$ initially: 1D, 2D with incident plane wave, and 2D with a Gaussian incident wave. For such a plasma, $k_{s1}\lambda_e = 0.38$; the linear ion Landau damping is weak, $\gamma_s/\omega_s \sim 0.003$; and the linear convective gain exponent for intensity is >150 for the incident plane wave. For the Gaussian beam the intensity at x=0 falls from its peak on the midline by 50% at the y boundary of the domain. Best focus occurs at $L_x/2$ and the midline in y where the wave intensity is 35% higher than where the laser enters at x=0. The power in the Gaussian beam was set equal to that for the incident plane wave case making the peak intensity of the Gaussian on the midline somewhat higher than for the plane wave. The Gaussian half-width in y for A_z at best focus in x is $1.5\lambda_0$. We note that the ion transit time laterally across the system for $9 \le ZT_e/T_i \le 16$, for which SBBS was significant, is comparable to the duration of the simulations for the baseline parameters. The peak SBBS reflectivities are high in all three cases in Fig. 3, and there is significant pump depletion. The 1D reflectivity remains high over the duration of the simulation ($\omega_s t \le 414 \sim 40 ps$), while the 2D reflectivities subside and are very weak by the end of the simulations. The peak Gaussian reflectivity is slightly higher than that for the plane wave, which we attribute to the higher pump wave intensity on the midline for the Gaussian. The initial ion temperature here is lower than that in Fig.1, which reduces the particle noise.

Figure 4 summarizes the results of simulations scanning a range of ZT_e/T_i values, which parameter controls the initial linear ion Landau damping and strongly influences

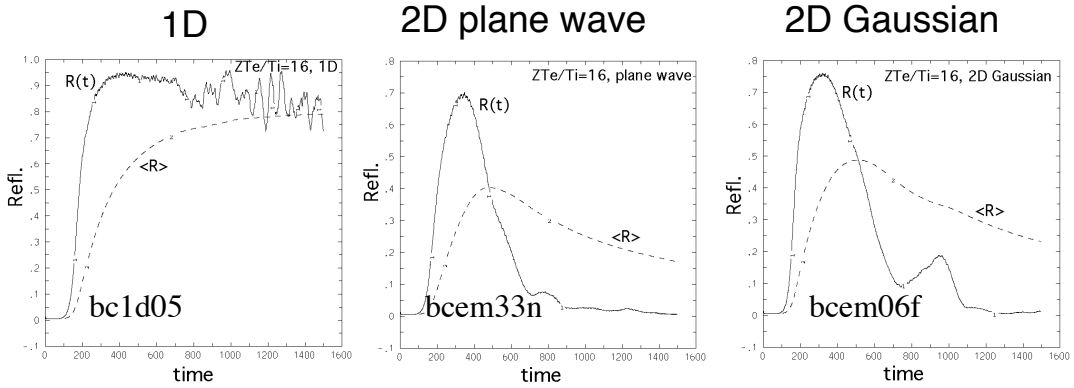

Figure 3. SBBS reflectivity time histories for three simulations: 1D, 2D plane wave, and 2D Gaussian beam.

the linear convective gain. The results shown here are some of the main results of the paper. The parameters for these simulations were the same as described in the beginning of Sec. IIA with $k_y=\pm(0,1,2,3)\Box 2\Box/L_y$ for the electromagnetic wave field and the full complement of 2D modes for the electrostatic potential. The dashed lines in Fig. 4a are the steady-state reflectivities determined by $R = \Box\exp G/(1+\Box\exp G)$ including pump depletion effects[23] where $\Box=(0.001/0.2)^2$ is the ratio of the seed and pump incident intensities and G is the linear intensity gain given by Eq.(4) which assumes that the ion wave is heavily damped. The 2D SBBS reflectivities are significantly smaller than those in 1D for $ZT_e/T_i \geq 6$.

We now address the detailed phenomenology exhibited by the simulations in order to understand the saturation processes. Ion trapping is evident when there is significant SBBS. Figure 5 shows ion velocity distributions $f_i(v_x)$ collected from the first third of simulation box and the corresponding phase-space scatter plots v_x vs. x for

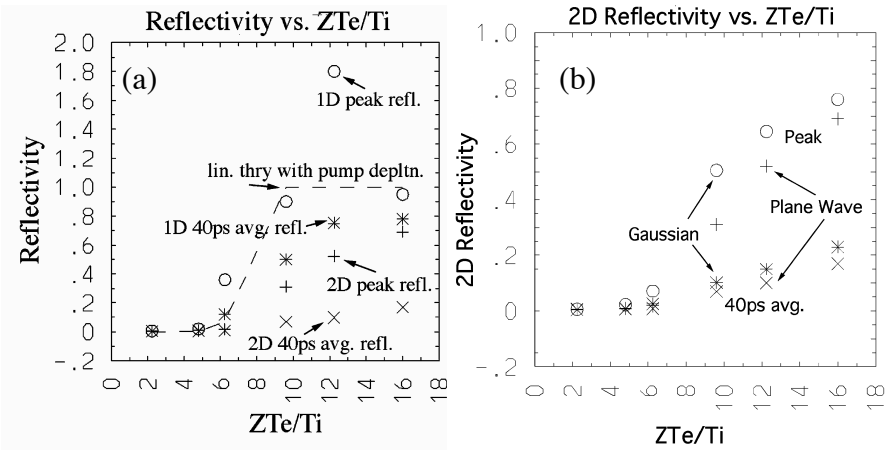

Figure 4. SBBS reflectivities in 1D and 2D (plane wave and Gaussian pump) as functions ZT_e/T_i. (a) 1D and 2D plane wave. (b) 2D plane wave and Gaussian.

simulations with $ZT_e/T_i = 16$ in 1D, 2D with a plane-wave laser, and 2D with a Gaussian-profile laser. Figure 6 shows that the ion trapping is spatially nonuniform and tracks the IAW amplification as expected. The IAW-produced distortions to $f_i(\mathbf{v})$ and concomitant spatially nonuniform detuning effects are observed to persist after the IAW amplitudes subside.[11] We observe transverse ion heating in 2D accompanying the saturation and relaxation of SBBS (Figure 7). The transverse ion heating is a consequence of the 2D scattering of the primary ion wave, which is expected if two-ion-wave decay and induced scattering of the IAW are occurring. The transverse ion heating contributes to the nonlinear dissipation of the SBBS ion wave. The simulations also exhibit evidence of IAW harmonic generation as a transient accompanying large SBBS IAW amplitudes (Fig. 8). This is particularly clear in 1D. The plots in Fig. 9 show the growth and saturation of the SBBS IAW measured at $x=L_x/4$ and Fourier analyzed in y. An obliquely propagating decay product grows up accompanying the decay of the primary SBBS IAW, which suggests that there is a secondary decay.

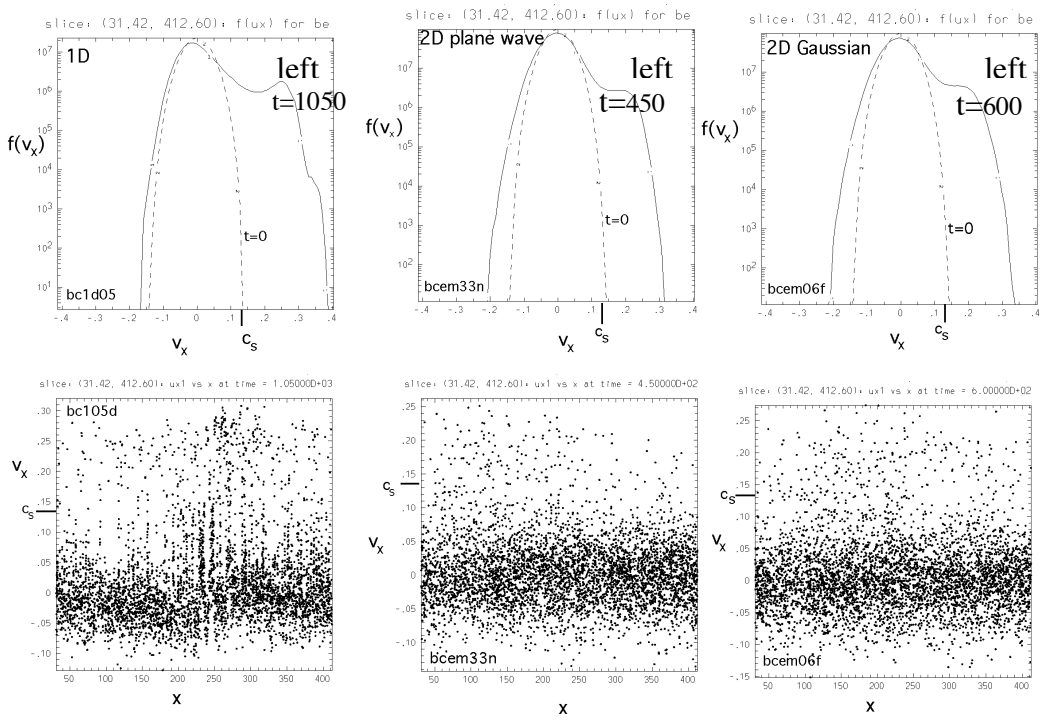

Figure 5. Longitudinal ion velocity distribution functions and phase space after saturation of SBBS in 1D, 2D with incident plane wave, and 2D with Gaussian beam. $ZT_e/T_i = 16.$

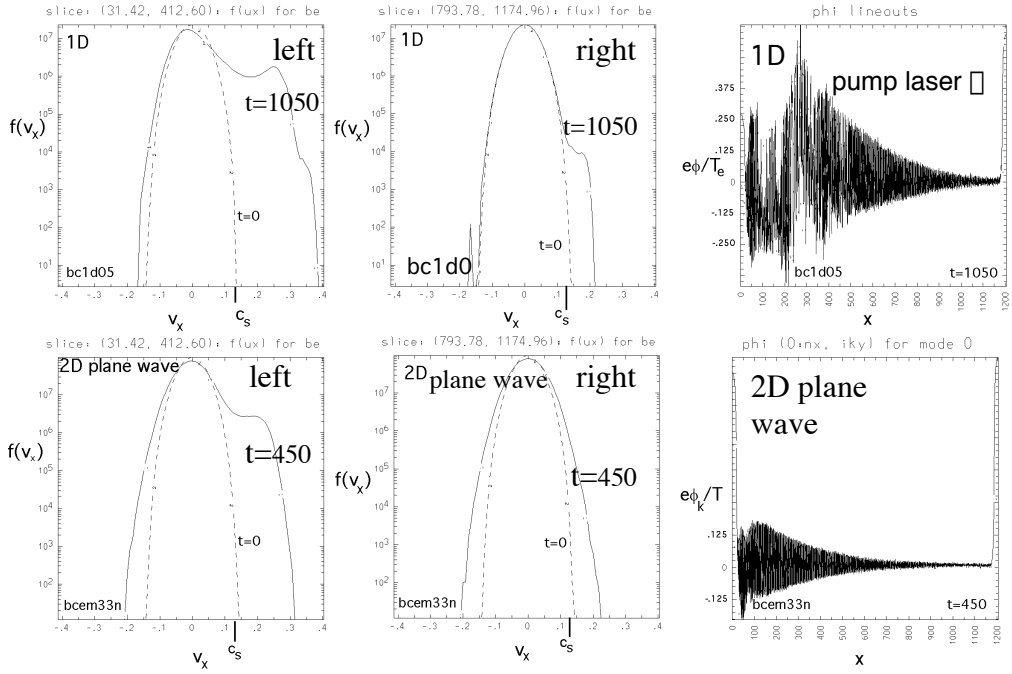

Figure 6. Longitudinal ion velocity distribution functions in the left and right thirds of the plasma domain and electric potential (k_y=0 in 2D) vs. x in 1D and 2D (plane-wave pump) after saturation of SBBS.

Accompanying the saturation and relaxation of the SBBS, we see a small bump emerge in $\left|\delta\phi(k_x,k_y)\right|$ in the 2D Fourier spectra near the subharmonic of the primary SBBS IAW with a small, but finite k_y, which suggests the two-ion-wave decay is occurring. The two-ion-wave decay spectrum in the simulations peaks near the primary SBBS IAW half-harmonic $0.5k_{SBBS} \sim k_0$ with a small $k_y \sim (0.2 \pm 0.1)k_0$, and the decay

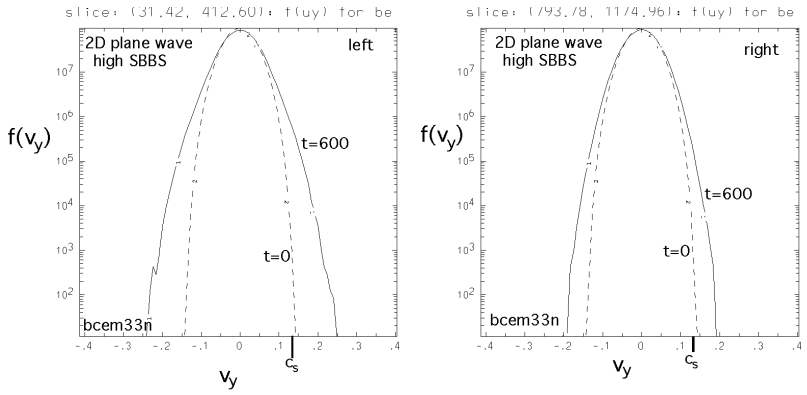

Figure 7. Transverse ion velocity distribution functions from the left and right thirds of the simulation domain after saturation of SBBS for a 2D plane-wave case with $ZT_e/T_i = 16$ showing heating.

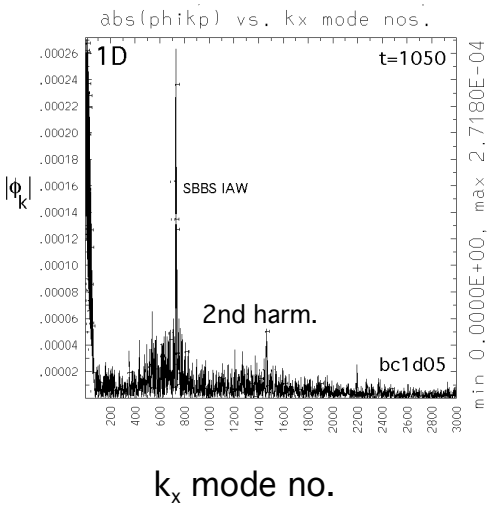

Figure 8. Spectrum $\left|\delta\phi_k\right|$ vs. k_x mode number for 1D simulation with $ZT_e/T_i = 16$ showing primary IAW and its harmonics after saturation. $\left\langle \left| e\delta\phi/T_e \right| \right\rangle_x \sim 0.1$ for the primary SBBS IAW at this time.

spectrum is broad: $0.7k_0 \lesssim k_x \lesssim 1.3k_0, 0.06k_0 \lesssim k_y \lesssim 0.4k_0$. The measurements reported in Ref. 22 do not fix the peak of the decay spectrum and determine only a lower bound on the width of the decay spectrum. Nevertheless, the bound on the experimental decay spectrum's relative width is similar to the spectral width in our simulations.

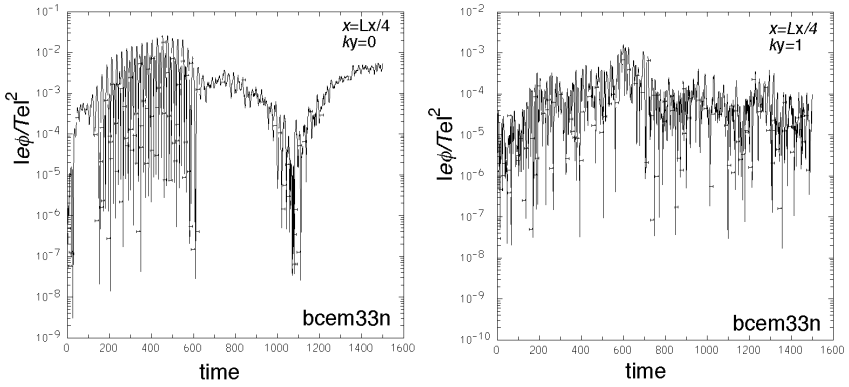

Figure 9. Plots of $\left|e\phi(x,k_y)/T_e\right|^2$ vs. time for the primary SBBS IAW with k_y=0 and the k_y=1 (in units of $2\pi/L_y$) mode showing the growth and decay of the primary IAW and the growth of the k_y=1 mode accompanying the decay.

We can corroborate some of the simulation features already identified and extract additional insights by post-processing the simulation data to produce streak spectra (Fourier amplitude vs. frequency and time) for the electromagnetic wave power flux and $\left|e\phi/T_e\right|^2$ at a probe location. The streak spectra are constructed from time histories of the fields using either a digital band-pass frequency filter or a running Fourier transform in time employing a moving data window. Figure 10 shows streak spectra for $\left|e\phi/T_e\right|^2$ at two different probe locations, backscatter and forward scatter electromagnetic fluxes on the midline at the left and right sides of the system, respectively, for the same 2D plane-wave simulation with $ZT_e/T_i = 16$ shown in Figs. 7 and 9. The streak spectra show the growth and relaxation of the primary SBBS IAW accompanying the backscatter signal.

As the SBBS relaxes we observe an IAW signal emerging at a frequency just below the subharmonic of the primary IAW, which corroborates the secondary decay in Fig. 9 and the appearance of a bump in the **k**-space spectrum near the subharmonic with small k_y,

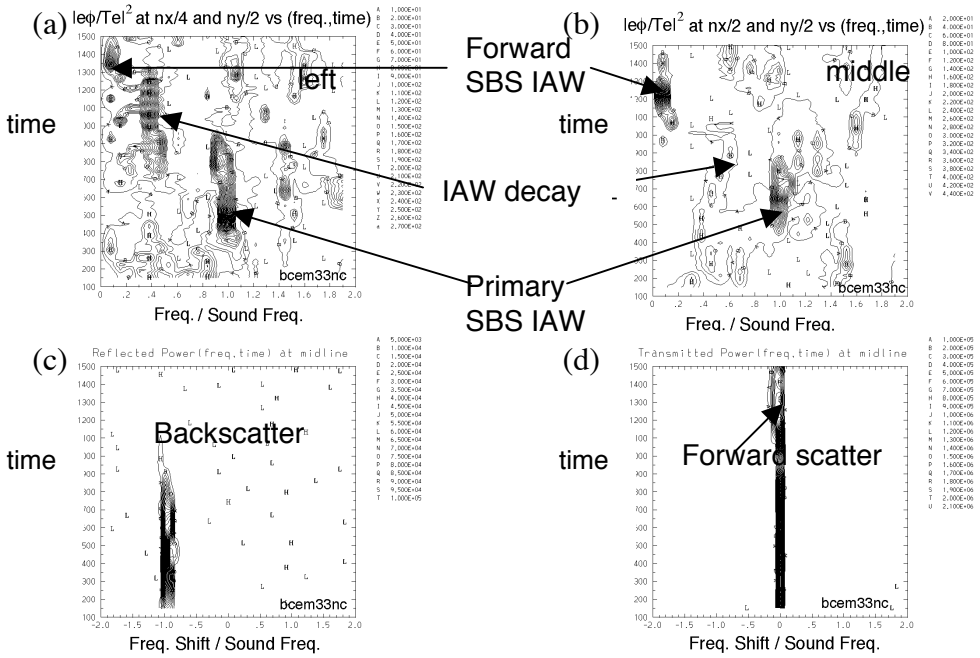

Figure 10. Streak spectra (contour plots of intensity vs. frequency relative to sound frequency of the primary SBBS IAW and time *t*) for $|e\phi/T_e|^2$ at two probe locations (a) and (b), and for the backscatter and forward scatter electromagnetic energy fluxes at the (c) left and (d) right system boundaries on the midline with $ZT_e/T_i = 16$.

and signifies the occurrence of the two-ion-wave decay. At late times a low-frequency IAW signal emerges accompanying the appearance of a slightly red-shifted feature in the forward scattered electromagnetic energy flux (Fig. 10d). Contour plots of $|A_z|$ vs. x/λ_x and y/λ_y at three different times in Fig. 11 show evidence of both backscatter and forward scatter later in time.

The emergence of forward SBS late in the 2D plane wave simulation with $ZT_e/T_i = 16$ raised the possibility that the long wavelength ion waves associated with forward SBS might contribute nonlinear dissipation by means of IAW mode coupling[14,24] that could help to explain the continued absence of SBBS at late times in the 2D simulations. Figure 12a shows the SBBS reflectivity for the 2D plane wave simulation

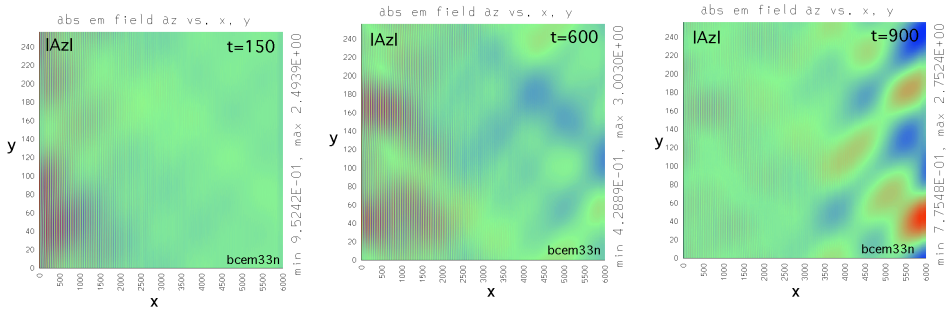

(a) Backward & Forward SBS (b) Backward SBS Only

Figure 11. Contour plots of $|A_z|$ vs. x/λ_x and y/λ_y at three times from the 2D plane-wave simulation with $ZT_e/T_i = 16$ showing backward SBS dominating on the left side of the system and later in time forward SBS dominating the right side.

with $ZT_e/T_i = 16$ shown in Figs. 7, 9-11 with backward and forward SBS occurring, and Fig. 12b shows the SBBS reflectivity with forward SBS suppressed by retaining only k_y=0. The peak SBBS reflectivities are similar, and the absence of significant SBBS for $t > 1000$ is the same in both simulations which suggests that IAW mode coupling involving the forward scattered ion waves was not the important mechanism in suppressing the SBBS late in time.

During the period of time when the SBBS reflectivities are crashing in the 2D simulations shown in Fig.12, inspection of the electrostatic mode amplitude time histories shows growth of obliquely propagating IAWs for both simulations with and without forward SBS (see Figure 13) and an enhanced level of energy compared to that in a 2D

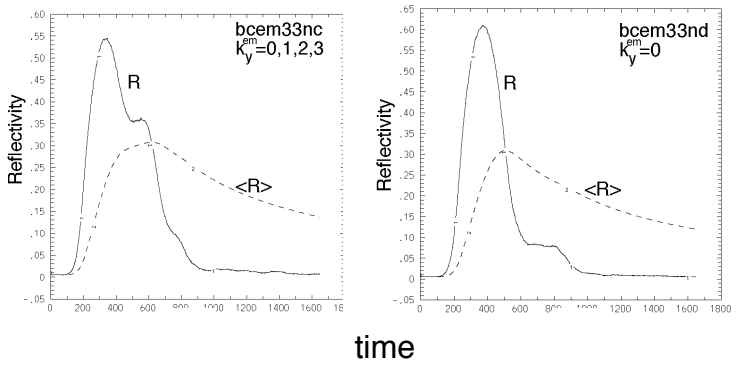

Figure 12 SBBS reflectivity for the 2D plane wave simulation with $ZT_e/T_i = 16$ (a) allowing both forward and backward SBS and (b) allowing only backward SBS.

simulation with no laser (which sets the thermal ion wave noise level for comparison). The scattering of the electrostatic energy from the primary SBBS IAW into oblique IAWs at longer wavelengths is accompanied by heating of the transverse ion velocity distribution $f_i(v_y)$ shown in Fig. 14. In the absence of SBS we observe no heating of $f_i(v_y)$. These simulation results suggest that two-ion-wave decay and NLLD of the primary SBBS IAW are important in cases of strong SBBS whether or not forward SBS is present.

We see from the simulation evidence presented that two-dimensional scattering of the SBBS primary IAW provides a mechanism for relaxing the primary IAW and causing the crash of SBBS. Subsequent to this the entire IAW spectrum is observed to relax and the 2D ion velocity distribution absorbs the energy. The 2D ion velocity distribution is heated transversely as well as longitudinally, and there is a pronounced hot-ion longitudinal tail produced. What then prevents the laser from re-exciting SBBS from the noise in this relaxed state? Our 2D simulations of strong SBBS show no signs of re-excitation. The nonlinear IAW dissipation from IAW mode coupling is much

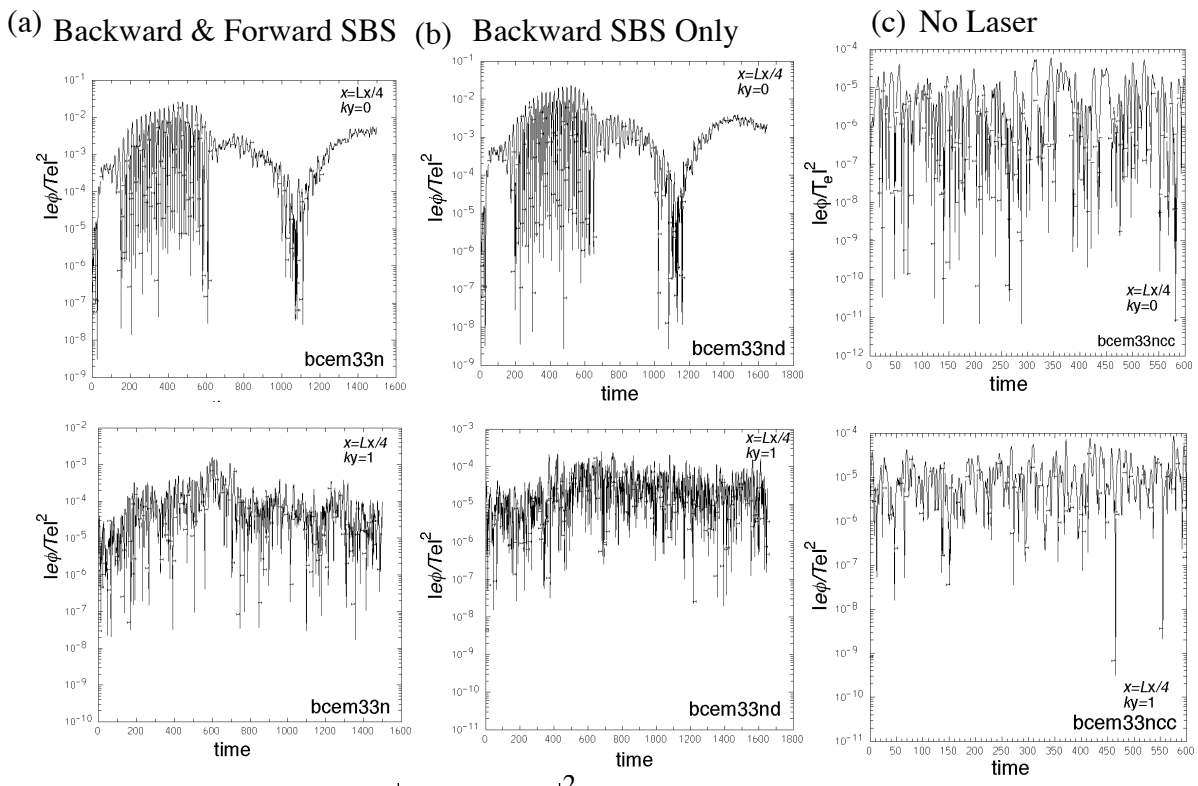

Figure 13. Plots of plots of $\left|e\phi(x,k_y)/T_e\right|^2$ vs. time for x=L_x/4 and k_y=0 or 1 (in units of 2π/L_y) for 2D plane-wave simulations with $ZT_e/T_i = 16$ in (a), with forward scatter suppressed in (b), and no laser in (c).

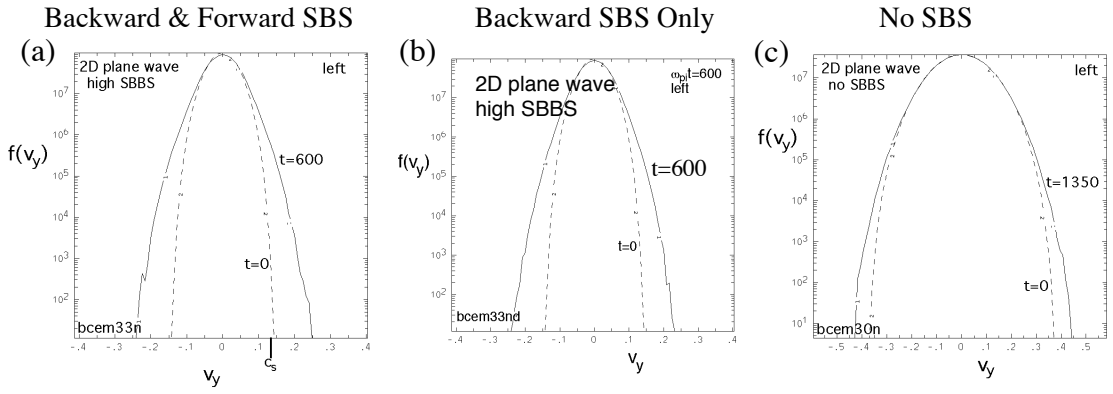

Figure 14. Transverse ion velocity distribution functions $f_i(v_y)$ corresponding to the three simulations shown in Fig. 13 showing significant transverse heating in the strong SBBS cases. $ZT_e/T_i = 16$ with strong SBBS in (a) and (b). $ZT_e/T_i = 2.24$ with no SBS in (c).

reduced in the relaxed state after the SBBS crash, but does IAW mode coupling still contribute to SBBS suppression? Furthermore, what level of IAW dissipation is supported by the modified $f_i(\mathbf{v})$? To investigate the crash and suppression of SBBS, and SBBS IAW dissipation due to the modified $f_i(\mathbf{v})$ in the 1D and 2D simulations that had exhibited strong SBBS, such as those shown in Fig. 3 ($ZT_e/T_i = 16$), we undertook several additional simulations in which we restarted the simulations after altering the conditions to address different questions.

When we restarted the 1D simulation in Fig. 3 at $t = 1500$ after scrambling the ion positions randomly over ~15 wavelengths λ_{SBBS} of the primary SBBS IAW (to quash and thermalize much of the existing IAW energy), turning off the incident pump laser and seed, and superposing a standing-wave IAW perturbation with $\delta n_i/n_i = 0.04$ at $k_x=2k_0$, the ensuing time history of $e\phi/T_e$ at a probe position $x=L_x/2$ was noisy, but showed no evidence of significant IAW damping. It should be kept in mind that Figs. 5 and 6 show that the 1D $f_i(v_x)$ as modified by ion trapping has a significant tail and regions where $df_i/dv_x>0$ for $v>c_s$. In contrast, when we restarted the 2D plane wave simulation shown in Fig. 3 at $t = 1650$ with the lasers off and an additional superposed ion wave perturbation with $\delta n_i/n_i = 0.02$, we saw evidence of the damping of the superposed IAW perturbation after the restart in (Fig. 15a). We note that the 2D $df_i/dv_x \leq 0$ for $v_x>0$ in Figs. 5 and 6. For reference we show in Fig. 15b the results of a simulation with the same parameters but with no lasers and no SBS.

We next restarted the 2D plane wave simulations with $ZT_e/T_i = 16$ shown in Figs. 14a and 14b after the crash and relaxation of the SBBS with the ion positions scrambled randomly over 15 λ_{SBBS} in x and ~2 λ_{SBBS} in y with the lasers on. The scrambling was

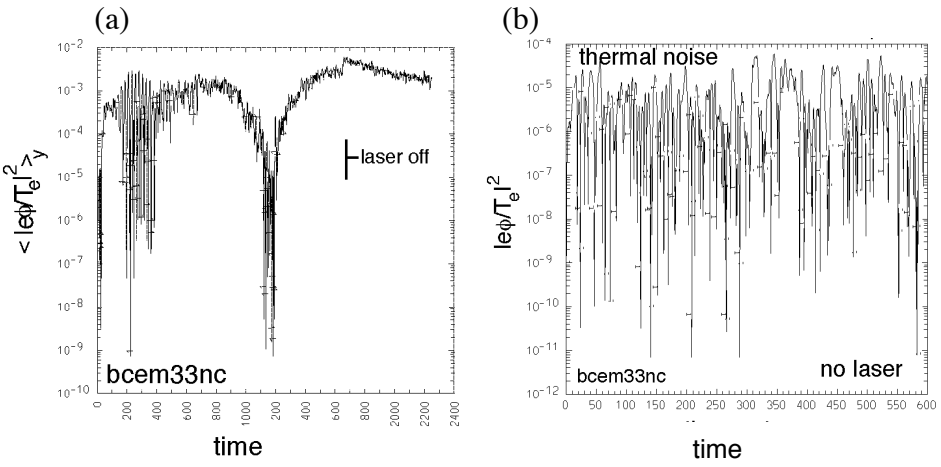

Figure 15. (a) Continuation of 2D simulation with $ZT_e/T_i = 16$ at $t/\tau t = 1650$ with lasers off and a $\delta n_i/n_i = 0.02$ perturbation added to study IAW damping. $\langle |e\phi/T_e|^2 \rangle$ at $x=L_x/4$ averaged over y vs. time. (b) Same as in (a) for simulation with no laser and no SBS.

(a) Backward SBS only

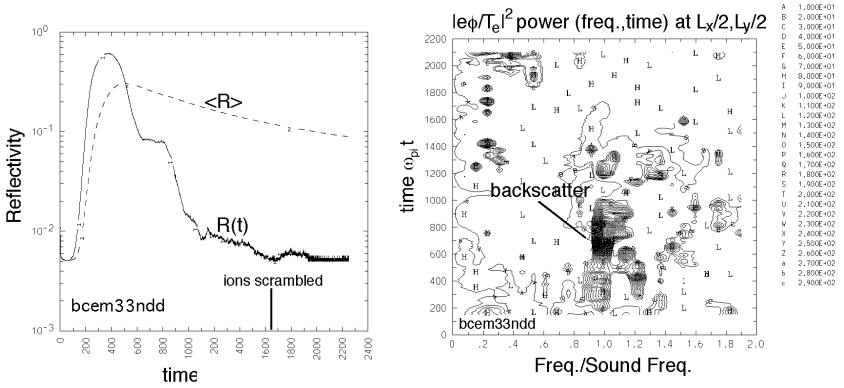

(b) Backward and forward SBS

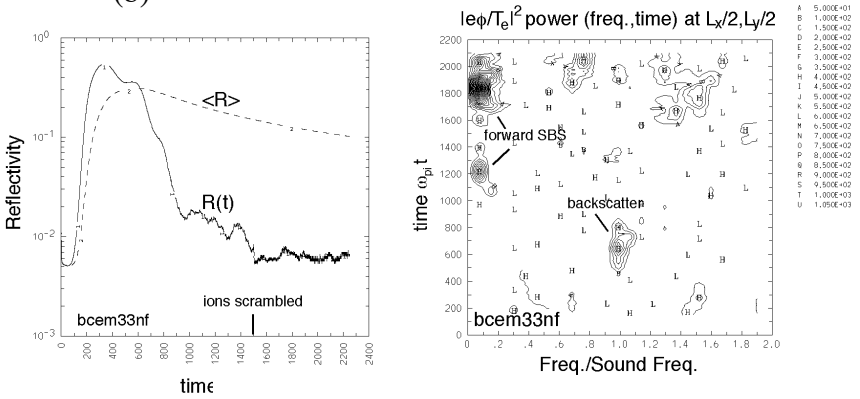

Figure 16. SBBS reflectivities vs. time and streak spectra for $|e\delta/T_e|^2$ at (L_x, L_y) for $ZT_e/T_i = 16$ (a) without and (b) with forward SBS showing that SBBS does not recover after scrambling ion positions and restarting.

intended to thermalize much of any residual coherent IAW energy in the system. The IAW energy levels before and after scrambling were comparable and well above Maxwellian $f_i(\mathbf{v})$ thermal levels. The forward SBS IAW (present in Fig. 14a) being much longer wavelength was unaffected by the scrambling. SBBS was not re-excited in either 2D simulation (with or without forward SBS, shown in Fig. 16). The electrostatic energy levels for these 2D plane wave simulations with $ZT_e/T_i = 16$ after the saturation and relaxation of SBBS given the significantly modified $f_i(\mathbf{v})$ is much increased over the levels in a 2D simulation with the same initial temperature but with no lasers and no SBS activity whatever (Figure 15). After SBS has relaxed and ions were scrambled or perturbed at $t \geq 1500$ as in Fig. 15a, $|e\phi(k_y=0)/T_e|$ was ~10× bigger than the thermal noise with no SBS and a 2D Maxwellian $f_i(\mathbf{v})$. The $|\delta n/n|^2$ levels are ~100× bigger for $k_y=0$ and ~5× bigger for $k_y=1,2$ in the SBS-active simulations after relaxation of the SBBS than the thermal noise levels with no SBS. We expect the thermal noise levels after the relaxation of SBS with the lasers turned off as in the simulation in Fig. 15a to be significantly enhanced over that in the unperturbed Maxwellian because of the heating, tail formation, and flattening of $f_i(v_x)$ near $v_x \sim c_s$. The theory of equilibrium thermal fluctuations in a plasma asserts that the thermal energy levels are $f/(df/dv_x)$ evaluated at the phase velocity of the IAW normal modes.[25] We are concerned with the thermal levels of the background ion waves in the SBS-active simulations because IAW mode coupling is a potential damping mechanism for the SBBS IAW and is proportional to $|\delta n_{\mathbf{k}}/n|^2$ summed over the background modes.[14,25]

Resetting the ion positions again in the bcem33nf simulation shown in Fig. 16b at t=2250 to uniform, quiet (regularly spaced) distributions in x and y decorrelated all ion

waves and removed the forward SBS IAW (Fig. 17). We note that $|\delta n/n|^2 \sim 0.8\times10^{-4}$ for $k_y\neq2$ after this second scrambling, which is ~4× the thermal noise of the unperturbed Maxwellian. The laser pump and seed remained on, and neither SBS backscatter nor forward scatter returned after the second scrambling. This supports the earlier result that the forward SBS is not assisting the continued suppression of SBBS.

The next two simulations discussed are especially revealing in elucidating why the 1D strong-SBBS simulations showed persistence of the backscatter while the corresponding 2D simulations exhibited a crash of the SBBS with no recovery. At

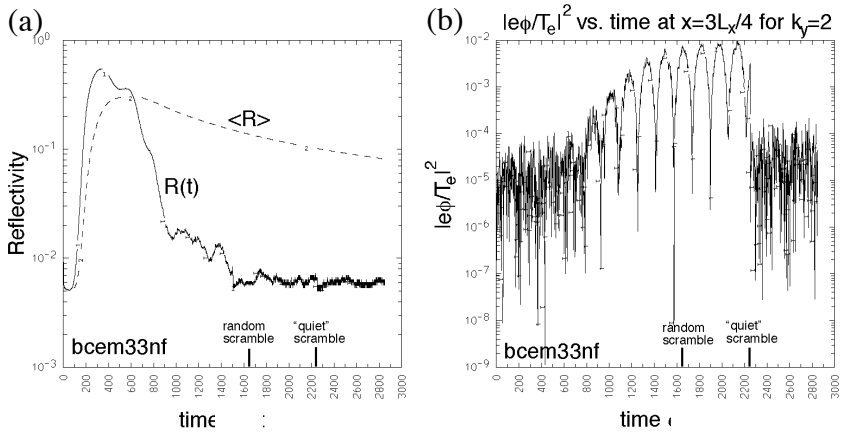

Figure 17. (a) SBBS reflectivity and (b) $|e\delta/T_e|^2$ at $3L_x/4$ for $k_y=2$ and $ZT_e/T_i=16$ vs. time with two restarts. The large amplitude IAW in (b) for $t\leq2250$ is associated with forward SBS.

t=300 in simulation bc1d05 (Figs. 3 and 5) we reset the ion positions to a quiet, regularly spaced distribution and set $A(\mathbf{x})=0$ and $\delta(\mathbf{x})=0$. The reset of the ion positions preserved the ion velocities and the strong spatial inhomogeneity of the modified $f_i(\mathbf{x},\mathbf{v})$ over the longest spatial scales. With the incident pump and seed lasers on ($v_{lhs}/v_e=0.2$, $v_{seed}/v_e=0.001$), SBBS backscatter and the primary IAW recovered and grew up from

small amplitudes in the restart (Fig. 18). The nonuniform, nonlinear frequency shift due to $f_i(\mathbf{x},\mathbf{v})$ was *insufficient* to limit the recovery of the backscatter here.[11]

The next simulation shows that the longitudinal ion velocity distribution $f_i(v_x)$ after the crash and relaxation of strong SBBS in 2D has sufficient dissipation to suppress SBBS in 1D. In this example, the spatial nonuniformity of the modified $f_i(v_x)$ was removed to isolate the effect of the Landau damping. We used as the initial condition in 1D the modified $f_i(v_x)$ from $[0,L_x/4]$ in 2D (bcem33n) at t=600 after SBBS backscatter

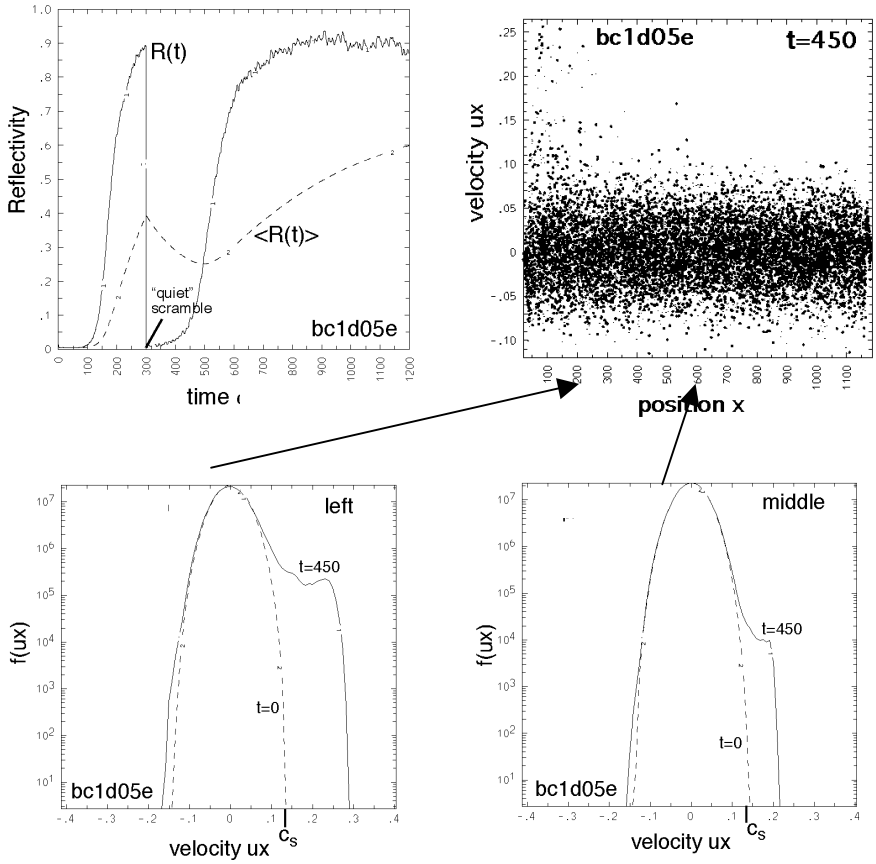

Figure 18. 1D simulation of SBBS with ZT_e/T_i=16 and a "quiet" reset of the ion positions at t=300 showing reflectivity vs. time; ion velocity phase space, and ion longitudinal velocity distribution functions in the left and middle thirds of the domain at t=450.

had saturated and then extended over $[0,L_x]$ in 1D with ion positions distributed uniformly. SBS backscatter did *not* grow to significant amplitude in this 1D simulation. Evidently the Landau damping in the modified $f_i(v_x)$ was sufficient to limit the backscatter. Although the slope of the 2D modified $f_i(v_x)$ was not nearly as negative near $v=c_s$ as in the initial Maxwellian, there were many more ions present because of the hot-tail formation. This result implies that any dissipation arising from 2D IAW mode coupling after the SBBS crashed was probably not the critical element in the continued suppression of SBBS. It also implies that the detuning due to the spatial nonuniformity

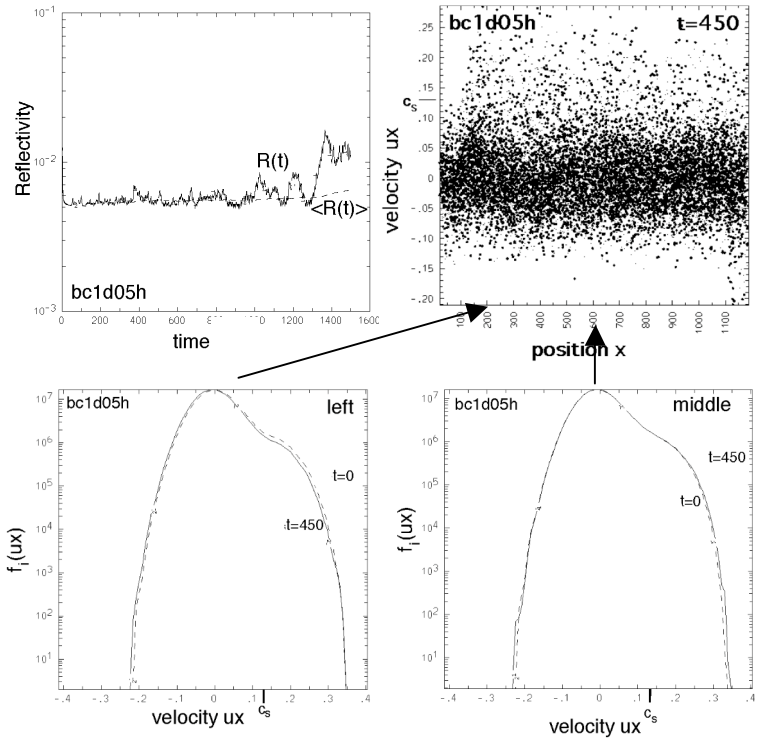

Figure 19. 1D simulation of SBBS with $ZT_e/T_i=16$ and initialized using the ion longitudinal velocities down-selected from $[0,L_x/4]$ in the 2D bcem33n simulation at $t=600$ after SBBS backscatter saturated and then extended over $[0,L_x]$ in 1D, showing reflectivity vs. time; ion velocity phase space, and ion longitudinal velocity distribution functions in the left and middle thirds of the domain at $t=450$.

of the trapped-ion modifications to $f_i(v_x)$ was not the critical element (which nonuniformity did *not* suppress SBBS in the 1D simulations shown in Figs. 3 and 18). Instead the simulation result shown in Fig. 19 indicates that the critical element in the continued suppression of SBBS in 2D was the dissipation provided by the modified $f_i(v_x)$ specific to the 2D simulations.

D. Ponderomotive Filamentation and Self-focusing

We noted that in the latter half of our 2D simulations with $ZT_e/T_i >> 1$ and strong SBBS there was appreciable forward scattering (Figs. 11, 16 and 17). In these simulations $L_y=16\lambda_0$ which was not large enough to allow ponderomotive filamentation according to Eq. (6). When we increased the box width to $L_y=48\lambda_0$ and left the other parameters unchanged, a 2D plane-wave simulation with $ZT_e/T_i=16$ exhibited filamentation (Fig. 20) following the crash of high levels of SBBS for $t<500$. The peak SBBS reflectivity exceeded 40%, crashed and relaxed to very small levels.

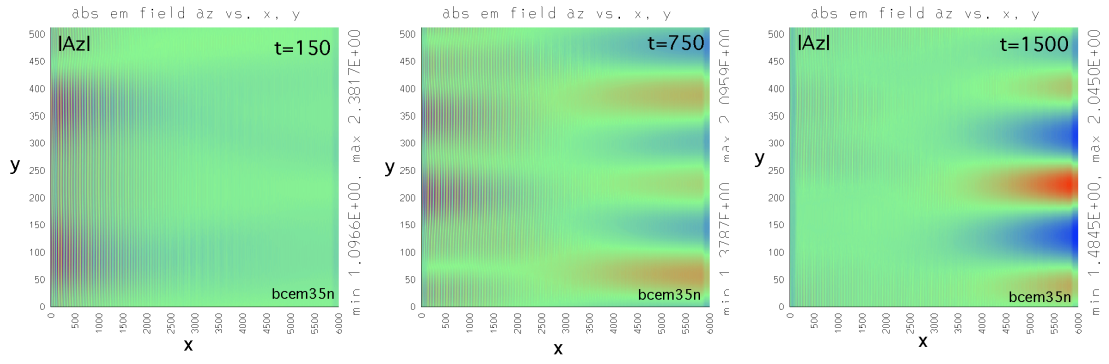

Figure 20. Color contours for $|A_z(x,y)|$ at three times (in units of $\omega_0 t$) showing the convective growth of ponderomotive filamentation with $ZT_e/T_i=16$.

For the 2D Gaussian-beam simulations and $ZT_e/T_i >> 1$, we observed high SBBS early in the simulations followed by evidence of ponderomotive self-focusing later in the simulations. The self-focusing is more severe with increasing values of $v_0^2/\left(v_e^2(1+T_i/ZT_e)\right)$ as the radiation pressure increases relative to the total plasma pressure.[26] Figures 21 and 22 show the results of simulations for different values of ZT_e/T_i with the self-focusing increasing with increasing ZT_e/T_i. The streak spectra in Fig. 22 show strong SBBS in the reflected signal and frequency spreading of the transmitted power accompanying the relaxation of the SBBS and self-focusing later in the simulation. The 2D plane-wave ponderomotive filamentation and 2D Gaussian-beam self-focusing observed in all cases are somewhat incidental to the SBBS given that the

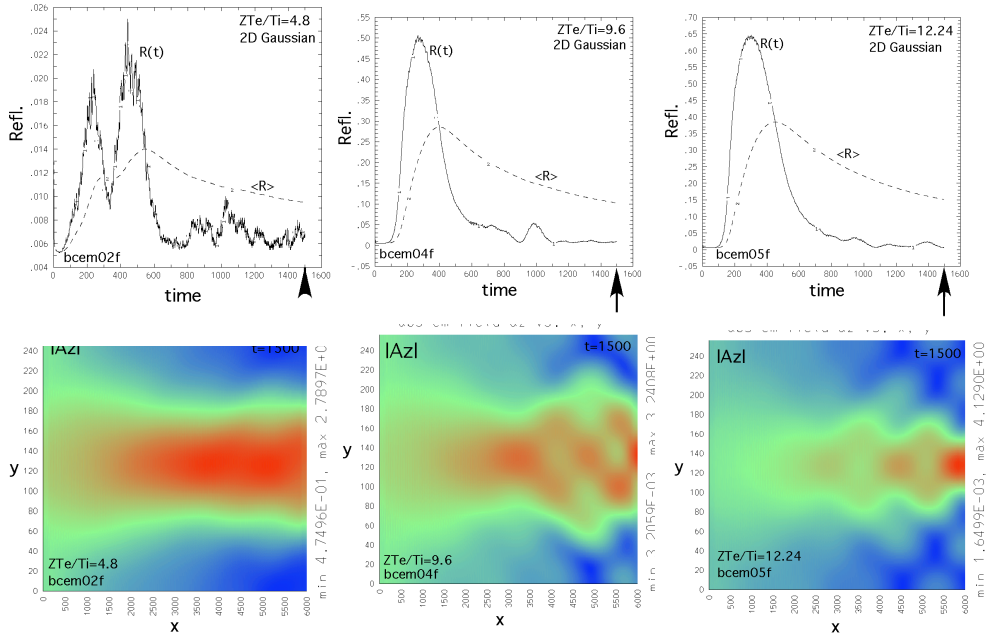

Figure 21. SBBS reflectivities vs. time t and color contours for $|A_z|$ vs. x and y at t/τ_0=1500 showing self-focusing in 2D Gaussian-beam simulations with baseline parameters: $L_x=192\lambda_0$, $L_y=16\lambda_0$, Be plasma (Z=4, A=9), m_h/m_e=1836, T_e=2 keV, v_0/v_e=0.2, n_e/n_c=0.1, N/cell=16, ZT_e/T_i=4.8, 9.6, and 12.24

SBBS dominates the early part of the simulations, saturates, and relaxes before the filamentation or self-focusing (or forward SBS) becomes significant. Of course, while the SBBS is large enough to severely deplete the pump laser, the convective growth of filamentation, self-focusing and forward SBS is significantly inhibited. Late in time in the 2D simulations when filamentation, self-focusing, or forward scattering is significant, the SBBS remains very weak.

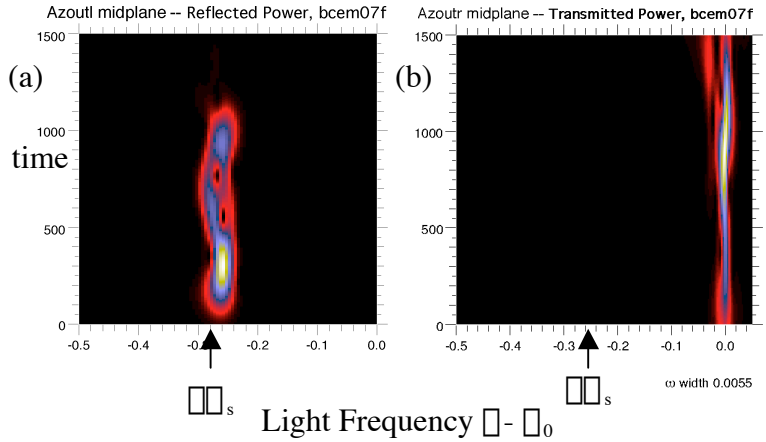

Figure 22. Streak spectra for electromagnetic (a) reflected power flux and (b) transmitted power flux vs. light frequency ω-ω_0 and time for a 2D Gaussian-beam simulation with ZT_e/T_i=16 and the baseline parameters listed in Fig. 21.

IV. CONCLUSIONS

1D and 2D hybrid simulations have been performed with the BZOHAR simulation code investigating the saturation of stimulated Brillouin backscattering (SBBS). Systematic scans of ZT_e/T_i for a Be plasma have been undertaken in 1D, in 2D with a plane-wave laser beam, and in 2D with a Gaussian-profile laser. Several nonlinearities contribute to the saturation of SBBS: ion trapping, wave breaking, pump depletion, two-ion-wave decay instability and nonlinear ion Landau damping, harmonic generation, and IAW mode coupling. The considerations in this work of the influence of

ion trapping on the saturation of SBS and the role of secondary instabilities involving the primary SBBS IAW parallel in many respects similar phenomena involving electron trapping and stimulated Raman scattering as expounded in the publication of Rose and Russell,[27] and in subsequent and ongoing research by H. Rose.

2D SBBS reflectivities saturate at significantly lower amplitudes than do SBBS reflectivities in 1D due to 2D nonlinear ion wave dissipation mechanisms, e.g., two-ion-wave decay and nonlinear ion Landau damping which lead to transverse and longitudinal ion heating. 2D reflectivities with Gaussian transverse laser profiles are higher than those from plane waves with the same incident power. High reflectivities recur in time in 1D, but not in 2D. Also, there is less flattening and tail formation in 2D compared to 1D. 2D mode coupling in enhanced 2D IAW turbulence can provide additional dissipation, but the overall importance of this IAW damping mechanism is unclear. It does not appear that IAW mode coupling is the critical element in accounting for the continued suppression of SBBS after the saturation and crash of SBBS. Instead the ion Landau damping in the 2D modified $f_i(v_x)$ is sufficient to suppress SBBS even when the spatial nonuniformity of the modified $f_i(x,v_x)$ is removed, because the modified longitudinal ion velocity distribution function in 2D that is self-consistent with low IAW amplitudes has finite negative slope and the hot-ion tail is well populated. The 1D physics lacks the nonlinear dissipation mechanisms that produce the crash of the SBBS in 2D, and the resulting BGK-like ion velocity distribution is self-consistent with a finite-amplitude IAW which in turn supports finite SBBS that persists in contrast to the 2D simulations.

After SBBS saturation for $ZT_e/T_i \gg 1$ there is evidence of whole-beam ponderomotive self-focusing for Gaussian beams, evidence of forward SBS for 2D plane

waves if the system is too narrow to admit filamentation, and evidence of filamentation for incident plane waves in wider systems. Of course strong SBBS occurring early in the simulations prevented simultaneous forward scattering instabilities of the laser by the simple means of depleting the pump. After SBBS crashed, the forward scattering instabilities had the opportunity to occur and no back-reaction on SBBS was observed.

Recent experimental work on stimulated Brillouin backscattering implies that nonlinearities such as ion trapping and secondary instabilities like the two-ion wave decay are relevant to understanding experimental observations.[21,22,28,29] However, the diagnostics in laser-plasma-interaction experiments are challenged to resolve the short timescales (<50 ps) in which the SBBS grows, saturates and crashes in a single speckle as suggested by simulations. On longer timescales the simulations need to incorporate collisions affecting the relaxation of the modified $f_i(\mathbf{v})$ which can presumably change the ion Landau damping left in the distribution function and impact SBS. In addition, on longer timescales the interaction of ions, electromagnetic waves, and ion waves in a volume interspersed with other active laser speckles should be incorporated in the simulations. These extensions are very significant challenges for kinetic simulation of SBS in multi-dimensions to be addressed in future work.

We gratefully acknowledge the many contributions to this effort and encouragement from Barbara Lasinski, Richard Berger, Dustin Froula, Siegfried Glenzer, Robert Kirkwood, Christoph Niemann, and Larry Suter. This work was performed under the auspices of the U.S. Dept. of Energy by the University of California Lawrence Livermore National Laboratory under contract No. W-7405-ENG-48.

References

[1]B.I. Cohen, B.F. Lasinski, A.B. Langdon, and E.A. Williams, Phys. Plasmas **4**, 956 (1997).

[2]B.I. Cohen, B.F. Lasinski, A.B.Langdon, E.A. Williams, K.B. Wharton, R.K. Kirkwood, and K. G. Estabrook, Phys. Plasmas **5**, 3408 (1998).

[3]C. Riconda, S. Huller, J. Myatt, and D. Pesme, Phys. Scr. T **84**, 217 (2000).

[4]E.A. Williams, Bull. Amer. Phys. Soc. **42**, 1998 (1997).

[5]D.W. Forslund, J.M. Kindel, and E.L. Lindman, Phys. Fluids **18**, 1017 (1975).

[6]W.L. Kruer, Phys. Fluids **23**, 1273 (1980).

[7]W.L. Kruer, *The Physics of Laser Plasma Interactions* (Addison-Wesley, Reading, MA, 1988).

[8]A. A. Andreev and V.T. Tikhonchuk, Sov. Phys. JETP **68**, 1135 (1989).

[9]H.X. Vu, J. Comput. Phys. **124**, 417 (1996); H.X. Vu, Phys. Plasmas **4**, 1841 (1997); R.E. Giacone and H.X. Vu, Phys. Plasmas **5**, 1455 (1998).

[10]E.A. Williams, B.I. Cohen, L. Divol, M.R. Dorr, J.A. Hittinger, D.E. Hinkel, A.B. Langdon, R. K. Kirkwood, D.H. Froula, and S.H. Glenzer, Phys. Plasmas **11**, 231 (2004).

[11]L. Divol, B.I. Cohen, E.A. Williams, A.B. Langdon, B.F. Lasinski, Phys. Plasmas **10**, 3728 (2003); L. Divol, R.L. Berger, B.I. Cohen, E.A. Williams, A.B. Langdon, B.F. Lasinski, D.H. Froula, and S.H. Glenzer, Phys. Plasmas **10**, 1822 (2003).

[12]J.A. Heikkinen, S.J. Kartunen, R.R.E. Salomaa, Phys. Fluids **27**, 707 (1984).

[13]K. Estabrook, W.L. Kruer, and M.G. Haines, Phys. Fluids B **1**, 1282 (1989).

[14]A.V. Maximov, W. Rozmus, V.T. Tikhonchuk, D.F. Dubois, H.A. Rose, and A.M. Rubenchik, Phys. Plasmas **3**, 1689 (1996).

[15]F. Detering, A. Heron, S. Huller, D. Pesme, C. Riconda, V.T. Tikhonchuk, "Kinetic Effects in the Nonlinear Evolution of a Driven Ion Acoustic Wave. Implications on Stimulated Brillouin Scattering," in Proceedings of the 34th Anomalous Absorption Conference, Salishan, OR, May 2004, 1O1.

[16]V.T. Tikhonchuk, private communication, 2004.

[17]B.I. Cohen and C.E. Max, Phys. Fluids **22**, 1115 (1979).

[18]J.D. Lindl, P. Amendt, R.L. Berger, S. G. Glendinning, S.H. Glenzer, S.W. Haan, R.L. Kauffman, O.L. Landen, L.J. Suter, Physics of Plasmas **11**, 339 (2004).

[19]P.W. Rambo, S.C. Wilks, and W.L. Kruer, Phys. Rev. Lett. **79**, 83 (1997).

[20]R.L. Dewar, Phys. Fluids **15**, 712 (1972).

[21]H.C. Bandulet, C. Labaune, K. Lewis, and S. Depierreux, Phys. Rev. Lett. **93**, 035002 (2004).

[22]C. Niemann, S.H. Glenzer, J. Knight, L. Divol, B.I. Cohen, C. Constantin, D.H. Froula, E.A. Williams, D.S. Montgomery, Phys. Rev. Lett. **93**, 0045004 (2004).

[23]C. L. Tang, J. Appl. Phys. **37**, 2945 (1966).

[24]B.I. Cohen, H.A. Baldis, R.L. Berger, K.G. Estabrook, E.A. Williams, and C. Labaune, Phys. Fluids **8**, 571 (2001).

[25]D.R. Nicholson, *Introduction to Plasma Theory* (John Wiley & Sons, NY, 1983), p. 219.

[26]C.E. Max, Phys. Fluids **19**, 74 (1976).

[27]H.A. Rose and D. Russell, Phys. Plasmas **8**, 4784 (2001).

[28]S.H. Glenzer, L. Divol. R.L. Berger, C. Geddes, R.K. Kirkwood, J.D. Moody, E.A. Willams, and P.E. Young, Phys. Rev. Lett **86**, 2565 (2001).

[29]D.H. Froula, L. Divol, and S.H. Glenzer, Phys. Rev. Lett. **88**, 105003 (2002); D.H. Froula, L. Divol, H.A. Baldis, R.L. Berger, D.G. Braun, B.I. Cohen, R.P. Johnson, D.S. Montgomery, E.A. Williams, et al., Phys. Plasmas **9**, 4709 (2002); D.H. Froula, L.Divol, D.G. Braun, B.I. Cohen, G. Gregori, A. Mackinnon, E.A. Willams, S.H. Glenzer, H.A. Baldis, D.S. Montgomery, et al., Phys. Plasmas **10**, 3728 (2003).